J Mater Sci (2010) 45:6701–6706
DOI 10.1007/s10853-010-4763-2

Structural and electrical conductivity studies on nanocrystalline undoped and silver doped zinc sulphide

S. Chellammal · S. Sankar · R. Murugaraj · S. Selvakumar · E. Viswanathan · K. Sivaji

Received: 7 October 2009 / Accepted: 9 July 2010 / Published online: 28 August 2010

Abstract Zinc sulphide (ZnS) and silver doped zinc sulphide nanocrystallites (ZnS:Ag) of average size 4 and 8 nm, respectively, have been synthesized by chemical precipitation technique. The structural and morphological studies using X-ray and high resolution transmission electron microscopy (HRTEM) measurements have confirmed hexagonal structure for the samples. Using the impedance spectroscopy method, the effect of grain interior and electrode–sample interface effect on their conductivity have been studied at various temperatures. In high temperature region, the electrode–sample interface effect is found to be larger than that of the grain interior region. Further, the results of the activation energies of the charge carriers in both the regions are determined and analyzed. The conduction mechanism of silver doped zinc sulphide nanocrystallites has been studied at various temperatures and the results are reported.

Introduction

A systematic study of size effect on the electrical properties of semiconducting nanocrystallites is essential for understanding their technological applications [1–3]. Nanocrystalline metal chalcogenides exhibit very interesting electronic structure and transition probabilities [4–6] and also many applications in the field of spintronics [7]. Among the II–VI semiconductors, zinc sulphide is widely studied owing to its stability and technological applications [8, 9]. Zinc sulphide nanoparticles doped with metallic elements has a variety of applications [10]. Several studies on the interesting optical properties of metal-doped ZnS nanoparticles have been reported in recent years [11–14]. However, studies on the characterization of electrical properties of metal-doped ZnS nanoparticles are seldom found. In this work, we report the electrical properties of pure and silver doped ZnS nanoparticles through impedance analysis.

Zinc sulphide is a direct band gap semiconductor with a band gap of $\sim$3.7 eV [14]. In this work, pure and silver doped ZnS (ZnS:Ag) nanocrystallites have been prepared by chemical precipitation method. X-ray characterization of the prepared nanocrystallites has been carried out for the confirmation of structure and also to obtain the average nanocrystallite size and these results are compared with the high resolution transmission electron microscopic (HRTEM) studies. The doping concentration of silver with ZnS was estimated by energy dispersive X-ray analysis (EDAX). Impedance measurements have been carried out in order to characterize the electrical properties of the sample over a temperature range from 573 to 873 K and the results are discussed and reported in this paper.

Experimental

Sample preparation

Chemical precipitation of silver doped ZnS nanocrystallites has been carried out at room temperature using the reactants

S. Chellammal · S. Sankar (✉)
Department of Physics, College of Engineering, Anna University, Guindy, Chennai 600025, Tamil Nadu, India
e-mail: ssankar@annauniv.edu; sankar_s52@yahoo.com

R. Murugaraj
Department of Physics, Madras Institute of Technology Campus, Anna University, Chennai 600044, Tamil Nadu, India

S. Selvakumar · E. Viswanathan · K. Sivaji
Department of Nuclear Physics, University of Madras, Guindy Campus, Chennai 600025, Tamil Nadu, India

anhydrous zinc chloride ($ZnCl_2$) and anhydrous sodium sulphide (Na_2S) with ethylene glycol as capping agent. Doping of silver was done by adding silver nitrate ($AgNO_3$) solution (0.005 M) with zinc chloride solution. The preparation was carried out over a reflux time of 600 s for 100 mL volume of the reacting solutions. The precipitate was then centrifuged and washed with de-ionized water repeatedly for several times and then finally with methanol. Then the precipitate was dried under vacuum for further studies.

Structural characterization

Powder X-ray diffraction studies were carried out using Mo Kα radiation ($\lambda = 0.070930$ nm) (Philip 2275/20 X-ray diffractometer) to determine the structural phase of the prepared samples. High resolution transmission electron microscopic (model: JEOL 3010 operated at 300 kV with a resolution of 0.14 nm) measurements were carried out to obtain the morphological characteristics of the samples. Energy dispersive X-ray analysis (EDAX) (Leo stereo scan 440 model) has been used to estimate the percentage of the dopant (Ag) content in ZnS:Ag nanocrystallites.

Electrical characterization

Complex impedance (|Z|, θ) measurements were carried out in a pellet of $\sim$8 mm diameter and $\sim$1.5 mm thickness as a function of frequency (from 1 Hz to 1 MHz) at different temperatures (from 573 to 873 K), by using an Impedance/Grain-Phase Analyzer (SOLARTRON 1260). Platinum electrodes were used for the impedance measurements.

The impedance analyzer is connected to a dedicated computer and software to acquire the impedance data. The whole setup of sample compartment inside the furnace was evacuated to 1×10^{-5} Torr, in order to prevent oxidation of sample during heating. The heating rate was maintained at 2 K/min. The temperature of the furnace was measured with a resolution of ±1 K using a Eurotherm (818 P) PID temperature controller. The impedance data collected during both heating and cooling cycles have been found to be highly consistent.

The conductivity (σ), the real (ε') and imaginary (ε'') parts of the dielectric constant (ε^*) as well as real (M') and imaginary (M'') parts of the complex modulus (M^*) were obtained from the relations:

$$c^*(\omega) = c'(\omega) - ic''(\omega) = 1/i\omega C_0 Z^*(\omega),$$

$$\sigma^*(\omega) = \sigma'(\omega) + i\sigma''(\omega) = i\omega c_0 c^*(\omega),$$

and

$$M^*(\omega) = M'(\omega) + iM''(\omega) = 1/c^*(\omega).$$

where ω is the angular frequency, $C_0 (C_0 = \varepsilon_0 A/d)$ is the vacuum capacitance, ε_0 is the free space dielectric permittivity, A is the cross-sectional area of the sample and d is the thickness of the sample.

Results and discussion

The powder XRD patterns of the synthesized nanocrystallites ZnS and ZnS:Ag samples are presented in Fig. 1a and b. The XRD pattern shows four peaks at 2θ values equal to 12.225, 20.625, 24.525 and 33.925 for ZnS sample and 13.045, 20.810, 24.578 and 32.954 for ZnS:Ag samples. The peaks have been identified to be due to the planes with the indices (1 0 0), (1 1 0), (2 0 0) and (2 1 1), respectively, of the hexagonal structural phase of ZnS (JCPDS PDF No: 011280) [15].

The present samples are prepared at room temperature (27 °C) while those of the earlier studies [8, 9] involved considerable heating of the reactants during preparation. The average grain size of the samples has been calculated from the powder XRD data using the Scherrer formula [16] as 4 nm for ZnS and as 8 nm for ZnS:Ag sample. Silver doped ZnS (i.e. ZnS:Ag) has its average size increased considerably when compared to that of ZnS by change in volume fraction. Depending upon the nature of dopant element, the volume fraction either increases or decreases [17]. In the present case, it is found that silver doping has the effect of increasing the average particle size of ZnS.

The HRTEM microstructures, lattice fringe patterns and electron diffraction rings of the nanocrystalline ZnS are shown in Fig. 2a–c and those for ZnS:Ag samples are

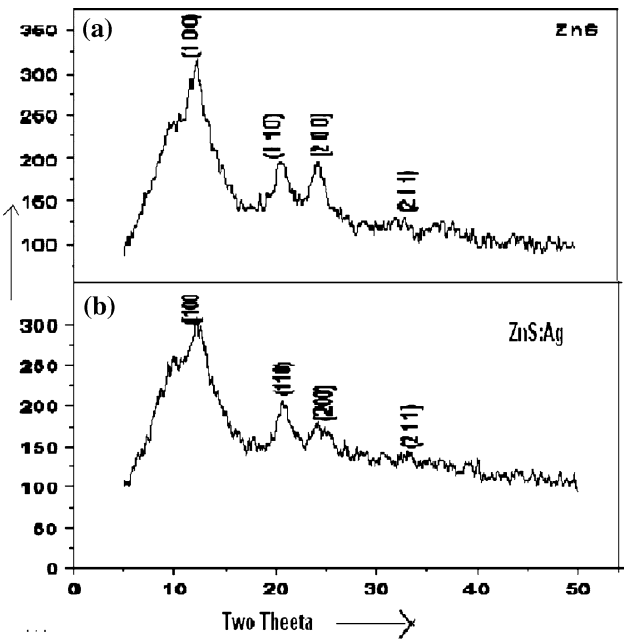

Fig. 1 Powder X-ray diffractograms of the as-prepared nanocrystalline (**a**) ZnS and (**b**) ZnS:Ag

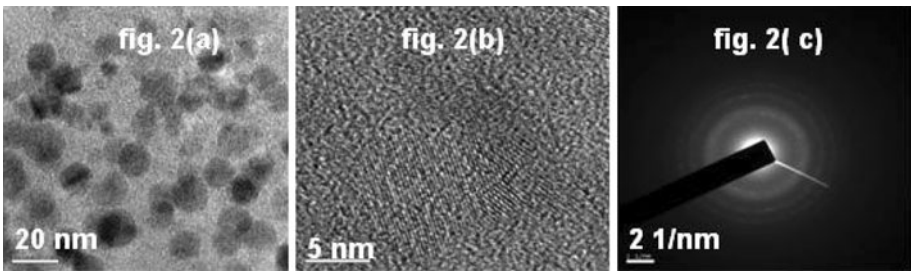

Fig. 2 **a** HRTEM microstructure, **b** lattice fringe pattern and **c** electron diffraction rings of nanocrystalline ZnS

presented in Fig. 3a–c, respectively. The HRTEM microstructures (Figs. 2a, 3a) show highly homogeneous size distribution in the ZnS sample, but the ZnS:Ag particles have very less homogeneity which is attributed to the presence of silver. In both the cases, the observed nanoparticles are nearly spherical. Their crystalline nature is evident from their lattice fringe patterns (Figs. 2b, 3b). The lattice planes yielding the rings of the selected area electron diffraction are indexed to (1 0 0), (1 1 0), (2 0 0) and (2 1 1) planes of the hexagonal phase of the samples. These results hence are in agreement with the X-ray diffraction studies.

The average size of the ZnS and ZnS:Ag nanocrystallites and their *d*-spacing values obtained by powder XRD studies for the samples are also compared with the corresponding sizes obtained from HRTEM measurements. It is worth pointing out here that, Borchert et al. [18] have demonstrated clearly that the average size of nanocrystallites can more reliably be obtained from XRD studies by Scherrer formula than the other size-measuring techniques such as HRTEM and small angle X-ray scattering (SAXS) studies.

In accordance with Borchert et al. [18], we have estimated the average size (d) of our present nanocrystallites samples using the Scherrer formula.

$$d = 0.9K\lambda/\omega\cos\theta \tag{1}$$

where the factor $K = 4/3$ accounts for the quasi-spherical geometry of the nanocrystallites, λ is the wavelength of X-rays used, ω is the width on 2θ-scale and θ is the scattering angle of X-rays. The above formula was also used by Nanda et al. [19] earlier to estimate the size of semiconductor nanocrystals consistently. Hence, we have also estimated the size of ZnS and ZnS:Ag nanocrystals in this work using the above formula (Eq. 1). The results indicate that silver doping has an effect of considerably increasing the average crystallite size and it is attributed to the doping of silver (Ag), since the conditions of sample preparation are identical for both the ZnS and ZnS:Ag samples. Due to change of volume fraction, the size of a particle has increased by the relation

$$\text{Volume fraction } = 1 - (1 - 1/d)^2 \tag{2}$$

where d is the size of a particle. This observation agrees well with that of Wang et al. [17] as mentioned earlier. The average size of the nanocrystallites and their *d*-spacing values obtained from the powder XRD studies are presented in Tables 1 and 2, for ZnS and ZnS:Ag samples, respectively, and are also compared with the corresponding sizes obtained from HRTEM studies. Table 3 shows the results of calculations of *d*-spacing by powder XRD and HRTEM studies and also theoretically using the equation

$$d_{hkl} = 1/\left(\left(h^2 + k^2 + hk\right)4/3a^2 + l^2/c^2\right)^{1/2} \tag{3}$$

for the prepared samples. The results of Table 3 confirm the hexagonal structure of the samples.

Table 1 Inter-planar spacing (d_{hkl}) and average grain size obtained by powder XRD and HRTEM studies for ZnS nanocrystallites

2θ (°)	(h k l)	d (Å)		Average grain size (nm)	
		XRD	HRTEM	XRD	HRTEM
12.225	(1 0 0)	3.31	3.30	4	4
20.625	(1 1 0)	1.92	1.92		
24.525	(2 0 0)	1.66	1.67		
33.925	(2 1 1)	1.33	1.32		

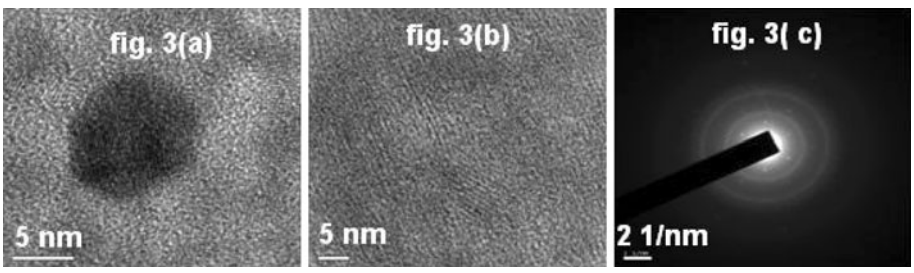

Fig. 3 **a** HRTEM microstructure, **b** lattice fringe pattern and **c** electron diffraction rings of nanocrystalline ZnS:Ag

Table 2 Inter-planar spacing (d_{hkl}) and average grain size obtained by powder XRD and HRTEM studies for ZnS:Ag nanocrystallites

2θ (°)	(h k l)	d (Å)		Average grain size (nm)	
		XRD	HRTEM	XRD	HRTEM
13.045	(1 0 0)	3.12	3.14	8	8
20.810	(1 1 0)	1.96	1.98		
24.578	(2 0 0)	1.67	1.68		
32.954	(2 1 1)	1.33	1.32		

Table 3 Experimental and theoretical inter-planer spacing (*d* values)

(h k l) planes	d-spacing			Parameters (Å)
	XRD (Å)	HRTEM (Å)	Theoretically (Å)	
(1 0 0)	3.31	3.12	3.14	$a = 3.811$
(1 1 0)	1.92	1.96	1.98	
(2 0 0)	1.66	1.67	1.68	$c = 6.234$
(2 1 1)	1.22	1.33	1.32	

Table 4 Activation energies for prepared ZnS and ZnS:Ag samples

Sample	Size (nm)	Activation energies (eV)	
		Defect phase (low temperature region)	Ordered phase (very high temperature region)
ZnS	4	1.71	3.64
ZnS:Ag	7	1.89	3.85

Energy dispersive X-ray analysis for the as-prepared ZnS and ZnS:Ag samples have yielded the percentage of the dopant (Ag) present as 1.04% (Table 4) in ZnS:Ag sample and shown in Fig. 4a and b for ZnS and ZnS:Ag, respectively.

In general, the three characteristic semicircular arcs of the impedance spectra represent the results for the high, intermediate and low frequency regions. These are correlated to grain interior regions, grain boundary regions of the sample and electrode–sample interface effects, respectively [20–23]. Figure 5a–c shows the impedance spectra for various temperature regions of ZnS sample.

Figure 6a–c shows the impedance spectra for various temperature regions of prepared ZnS:Ag sample. At low temperature region, that is 350–400 °C, the resistance varies from 1.35×10^5 ohm to 7088 ohm and the relaxation time changes from 4×10^{-6} to 1.4×10^{-7} s for ZnS:Ag sample. In this temperature region, single semicircular arcs only were observed as shown in Figs. 5a and 6a. Hence the relaxation times of grain and grain boundary regions are almost equal and so all of the semicircular arcs merge together showing single relaxation time. In this region, a low conductivity is observed in the sample.

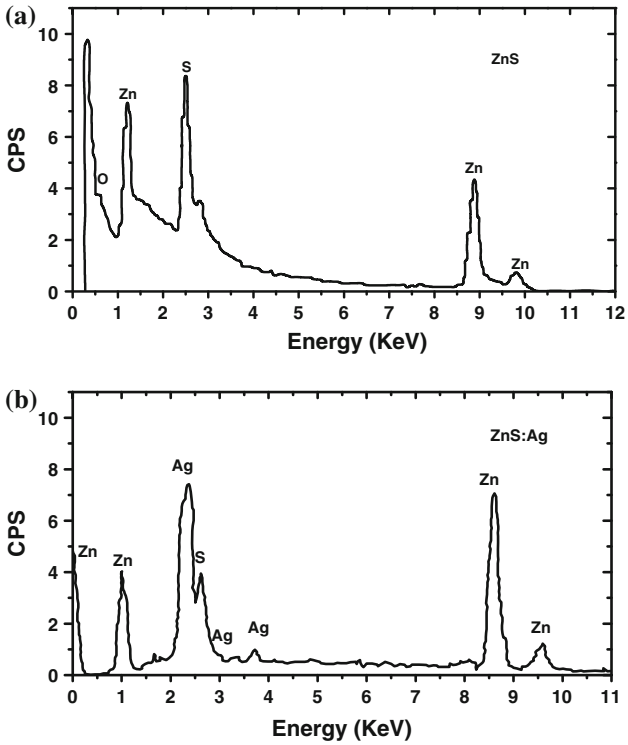

Fig. 4 **a**, **b** EDAX pattern for ZnS and ZnS:Ag samples

As the temperature is further increased, from 430 to 450 °C, the resistance value of grain is found to be decreased from 2194 to 2142 ohm and the corresponding relaxation time changes from 2.5×10^{-8} to 2.3×10^{-8} s for ZnS:Ag sample. Figure 6b shows one semicircular arc with a straight line and it implies that the arc represents the presence of relaxation process in the grain boundary as reported by Biju et al. [24] and the straight line indicates the presence of electrode–sample interface effect.

It has also been observed that the conduction increases while increasing the temperature. But the relaxation time decreases with increase in temperature. This observation indicates that the grain boundary disorders decrease thereby enhancing the grain–grain interaction as temperature increases.

At still higher temperature region, 450–480 °C, the resistance values have decreased considerably, from 2142 to 254 ohm, but the relaxation time has been observed to be almost constant equal to $\sim 2.53 \times 10^{-8}$ s for ZnS:Ag sample. In this region, the conduction increases considerably without any appreciable change in the relaxation time as the temperature increases. Figures 5c and 6c show that there exists only a single arc and it is attributed to the effect of grain boundary. The straight line at the low frequency implies the electrode–sample interface effect which is present even at high temperature.

Figure 7a and b show the conductivity of the sample at different temperatures. They reveal the grain contribution mechanism. At very high temperature region (above

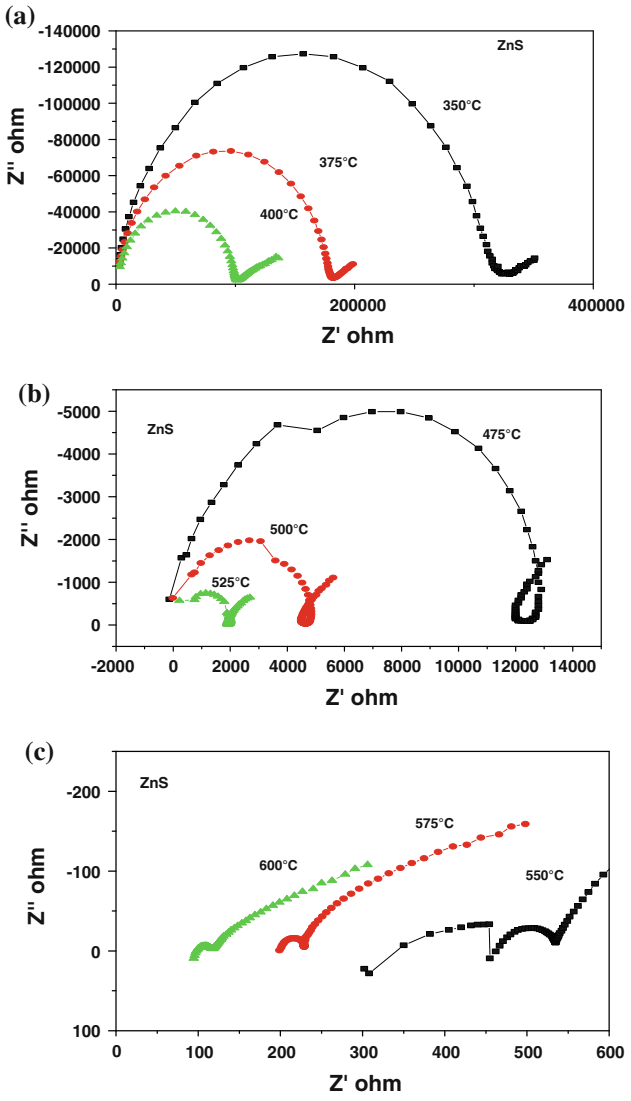

Fig. 5 a–c Impedance spectra at different temperatures for ZnS sample

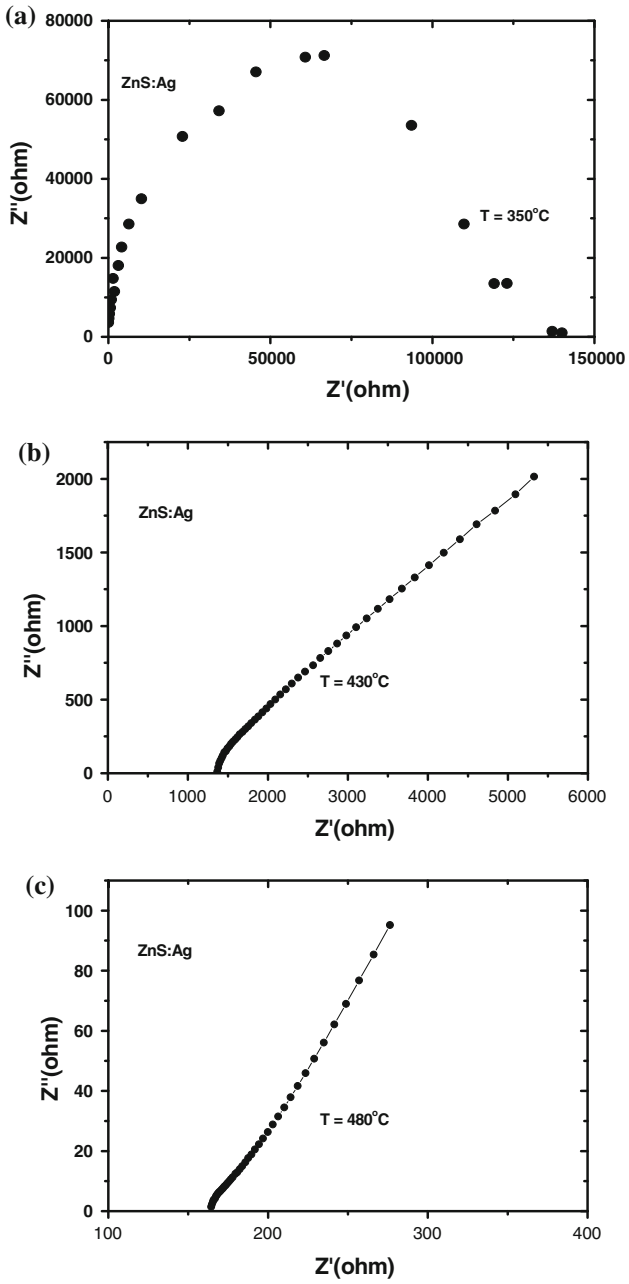

Fig. 6 a–c Impedance spectra at different temperatures for ZnS:Ag sample

430 °C), the conduction process may be attributed to the conduction across the grain boundaries and the low temperature (below 350 °C) conduction process may be attributed to the conduction within the grains. Figure 7a and b illustrates the increase in the activation energy with respect to temperature thereby reflecting the blocking nature of the grain boundaries and also show the increase in activation energy at very high temperature (above 430 °C).

The activation energies as calculated from Fig. 7a and b, are 1.71, 3.64 eV for ZnS and 1.89, 3.85 eV for ZnS:Ag nanocrystallites as shown in Table 4. The activation energy is increasing at very high temperature owing to the larger grain interface. The increase in conductivity with the increase in temperature implies that the defect density decreases [20]. The prepared nanoparticles may contain open volume defects including vacancies. On heating, considerable decrease in the concentration of these defects can be expected which in turn might give rise to an enhancement in the crystalline or more ordered phase of the sample. Figure 7a and b shows the above mentioned phase transition by the change in the slope in Arrhenius plot at ~400 °C.

Conclusion

In this work, pure ZnS and Ag doped ZnS nanocrystallites have been prepared by chemical precipitation method with

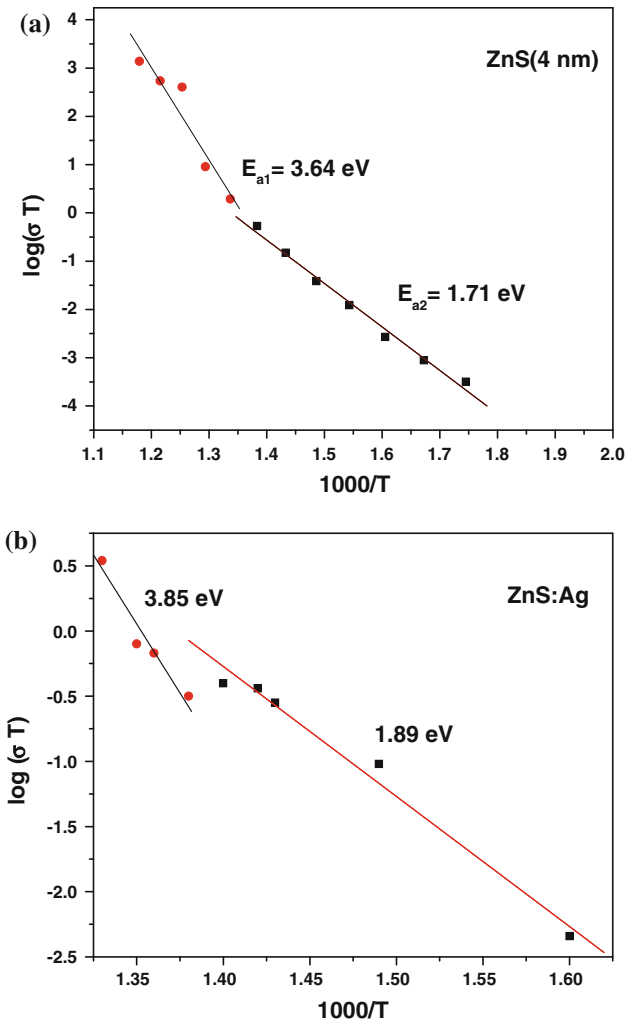

Fig. 7 **a**, **b** Arrhenius plots for ZnS and ZnS:Ag samples

average crystallite sizes of 4 and 8 nm, respectively. The XRD and HRTEM measurements confirmed the hexagonal structure of the samples. The effect of electrical conduction through grain boundary and electrode–sample interface effect at different temperature ranges have been studied through impedance spectroscopy method. The relaxation process associated with the grain boundary region of the nanocrystallites is identified. We observed that the conduction process through the grain boundary regions exceeds the conduction across the inter-granular regions. At high temperature, impedance analysis describes that the conduction relaxation process across the grain boundaries is saturated. At very high temperature, the increase in activation energy from 1.89 to 3.85 eV is attributed to the presence of large grain interface. The phase transition indicated by the Arrhenius plots may be ascribed to the transition from a defective phase to a more crystalline phase of the samples.

References

1. Chen S, Liu W (1999) Langmuir 15:810
2. Nanda J, Sapra S, Sarma DD (2000) Chem Mater 12:1018
3. Chestnoy N, Hull R, Brus LE (1986) J Chem Phys 85:2237
4. Norris DJ, Yao N, Charnock FT, Kennedy TA (2001) Nano Lett 1:3
5. Chen W, Malm JO, Zwiller V, Huang Y, Liu S, Wailenberg R, Bovin JO, Samuelson L (2000) Phys Rev B 61:11021
6. Soo YL, Ming ZH, Huang SW, Kao YH, Bhargava RN, Gallugher D (1994) Phys Rev B 50:7602
7. Awschalom DD, Kikkawa JM (1999) Phys Today 52:33
8. Geng BY, Zhang LD, Wang GZ, Xie T, Zhang YG, Meng GW (2004) Appl Phys Lett 84:2157
9. Bhattacharjee B, Ganguli D, Iakoubovesku K, Stesmans A, Chaudhuri S (2002) Bull Mater Sci 25:175
10. Nanda J, Kuruvilla BA, Sarma DD (1999) Phys Rev B 59:7473
11. Fisher AG (1963) J Electrochem Soc 110:733
12. Mu J et al (2005) Mater Res Bull 40:2198
13. Lee S, Song D et al (2004) Mater Lett 58:342
14. Huang J, Yang Yi, Xue Shanhua et al (1997) Appl Phys Lett 70:2335
15. Fuller ML (1929) Philos Mag 8 (658), version 2.3V
16. Cullity BD (1978) Elements of X-ray diffraction, 2nd edn. Addison-Wesley, Reading, MA
17. Wang M, Sun L, Fu X, Liao C, Yan C (2000) Solid State Commun 115:493
18. Borchert H, Shevchenko EV, Robert A, Mekis I, Kornowski A, Grubel G, Weller H (2005) Langmuir 21:1931
19. Nanda J, Kuruvilla BA, Sarma DD (1999) Phys Rev B 59:7473
20. Macdonald R (ed) (1987) Impedance spectroscopy, emphasizing solid materials and systems. John Wiley, New York
21. Cole KS, Cole RH (1941) J Chem Phys 9:341
22. Almond DP, West AR (1983) Solid State Commun 9, 10:277
23. Sinclair DC, West AR (1989) J Appl Phys 66:3850
24. Biju V, Abdul Khadar M (2001) Mater Sci Eng A 304–306: 814